Electro-optic characteristics of a transparent nanophotonic device based on carbon nanotubes and liquid crystals

Ranjith Rajasekharan, Qing Dai, and Timothy D. Wilkinson*

Department of Engineering, Centre of Molecular Materials for Photonics and Electronics, University of Cambridge, 9 J. J. Thomson Avenue, Cambridge CB3 0FA, United Kingdom

*Corresponding author: tdw13@cam.ac.uk

We present electro-optic characteristics of a transparent nanophotonic device fabricated on quartz substrate based on multiwall carbon nanotubes and nematic liquid crystals (LCs). The nanotube electrodes spawn a Gaussian electric field to three dimensionally address the LC molecules. The electro-optic characteristics of the device were investigated to optimize the device performance and it was found that lower driving voltages were suitable for microlens array and phase modulation applications, while higher driving voltages with a holding voltage can be used for display-related applications.

OCIS codes: 230.0230, 230.3720, 350.4238, 350.4600.

1. Introduction

The electro-optic characteristics of carbon nanotubes (CNTs) doped in liquid-crystal (LC) cells have been studied [1–6]. A change in threshold voltage and response time was observed due to suppression of field screening effect and increase in LC dielectric anisotropy induced by incorporating CNTs [6]. We have demonstrated nanotubes as an electrode site to three dimensionally address the LC molecules and, hence, an electrically switchable nanophotonic device based on a sparse array of multiwall CNTs (MWCNTs) grown on a silicon surface [7]. The nanotube electrodes were grown vertically on silicon substrate. (perpendicular to the plane of silicon substrate). The device operated in reflective mode. The Gaussian electric-field profile from nanotube electrodes [8] dictated the refractive index profile across the device. The refractive index profile then acted as a series of graded index profiles, which form a simple phase modulating element [9]. By varying the external electric field applied, it was possible to tune the properties of this graded index structure. In this paper, we report electro-optic characterization and optimization of a new nanophotonic device where the nanotubes were grown vertically on a quartz substrate. The device operated in transmission mode. The transparent device has an advantage of making compact electro-optic devices with less alignment complexity. The response time, contrast ratio, and phase modulating power of the nanophotonic device were studied at different operating voltages. A step-voltage driving scheme was used to eliminate the optical bounce and effectively improve the rise time and fall time of the device. The device applications were proposed based on the variation of applied electric field, which showed that lower driving voltages were suitable for microlens array and phase modulation applications, while higher driving voltages with a holding voltage can be used for display applications.

Figure 1 shows a transparent nanophotonic device with nanotubes attached vertically to the lower electrode and an upper electrode acting as an earth plane for the electric field. The lower electrode was made of quartz substrate with a 100 nm thick titanium

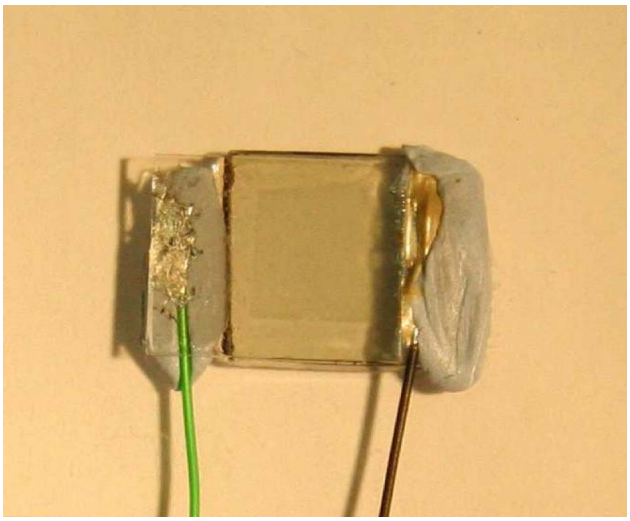

Fig. 1. (Color online) CNT and LC based transparent nanophotonic device.

nitride layer for electric contact, and the upper electrode is indium tin oxide on 0.5 mm thick borosilicate glass. The cell gap was set to 20 μm using spacer balls in UV glue and was filled with nematic LC BL048 from Merck. The top electrode alone was given a planar alignment by rubbing a thin film of polyimide (AM4276) and, hence, the resultant alignment of the device was hybrid. In the current device, the nanotubes were patterned in small groups of six with a 1 μm spacing between the nanotubes and 10 μm spacing between the groups to increase the resultant electric field and, hence, the diameter of each phase modulating element, as shown in Fig. 2.

2. Electro-Optic Characteristics of the Nanophotonic Device

A. Transmission Voltage Characteristics

A He–Ne laser (633 nm) was used to characterize electro-optic properties of the nanophotonic device. The device was placed between a crossed polarizer and analyzer with a rubbing direction 45° to the polarizer axis. Figure 3 shows the transmission (T) versus voltage (V) curve for the device, along with images of device switching at 0, 3, and 4.5 V_{rms}. The T–V curve goes through several maxima and minima as the applied voltage increased from 0 to 15 V_{rms}, and it attained a lower limiting value at higher voltages. This is because the nanophotonic device acted as a phase retardation plate. The maximum value of measured phase retardation from the T–V characteristics is 16π for the transparent device. This can be further explained using voltage-dependent director orientation of LC molecules. The rodlike nematic LC molecules in the device align parallel to a preferred direction specified by the director vector. When the laser beam propagates through the planar aligned LC cell device with its polarization axis at an angle of 45° to the director orientation (rubbing direction), ordinary rays (n_o) and extraordinary rays (n_e) in the outgoing beam experience a phase difference δ [10]:

$$\delta = \frac{2\pi d \Delta n}{\lambda} \sin^2 \theta, \tag{1}$$

where d is the cell thickness, $\Delta n (n_e - n_o)$ is the birefringence of the LC, λ is the wavelength, and θ is the angle between the optic axis of the LC and the light propagation direction. From the optical phase difference, the transmitted intensity through the device between the crossed polarizer and analyzer can be represented as $I_\perp$:

$$I_\perp = I_o \exp(-\alpha_0 d) \sin^2 \frac{\delta}{2}, \tag{2}$$

where I_o is the incident beam intensity and α_0 is the LC absorption coefficient for the ordinary ray. The reason for the maxima and minima in the transmission curve is that the LC molecules are oriented by the applied electric field, which changes the phase of the outgoing ordinary and extraordinary rays and, hence, creates changes in optical retardation, as given in Eqs. (1) and (2). The transmitted intensity was minimum for the device at higher voltages because of homeotropic alignment of LC molecules at nanotube positions. The alignment of the device was studied further by rotating the device from 0° to 360° between the crossed polarizer and analyzer. The align-

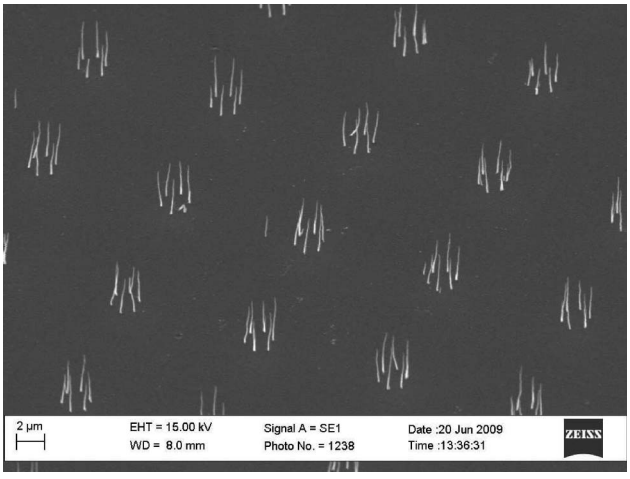

Fig. 2. Transmission electron microscope image of multiwall CNT electrodes on quartz.

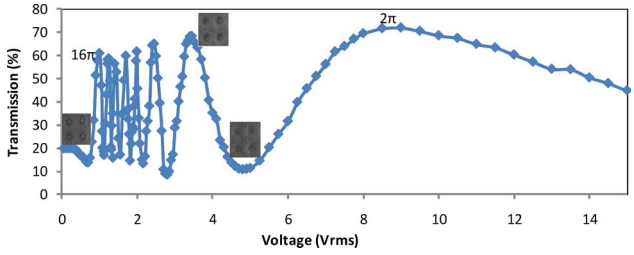

Fig. 3. (Color online) T–V characteristic of the transparent nanophotonic device along with an image of the device switching at 0, 3, and 4.5 V_{rms}.

ment at 0 and 3 V_{rms} is shown in Fig. 4. It was clear from the analysis that the Gaussian electric field from the CNT gave a more horizontal component of electric field at lower voltages and, hence, planar alignment predominated over the device, which resulted in an increased transmission at lower voltages compared to decreased transmission at higher voltages because homeotropic alignment predominated [10,11].

B. Response Time of the Device

The response time of a LC device is important for making applications. When an external electric field is applied, the field induces external torque to each molecule, which leads to fast switching. But when the voltage is removed or reduced, interaction between LC molecules provides the major restoring forces and these forces are much weaker than the external-field-induced torque and hence slow switching time. The response time varied from 1.57 s to 125 ms for different voltages for BL048 nematic LCs with a cell gap of 20 μm [12]. The nanophotonic device was characterized using a He–Ne laser of wavelength 633 nm to measure the response time. Driving electronics were developed to make a holding voltage (bias voltage) to drive the device from different voltage levels using a counter, an analog switch, and logic gates. The device was placed between the crossed polarizer and analyzer with the rubbing direction 45° to the transmission axis. A voltage pulse of 3.12 V_{rms} without any holding voltage was used here to drive the device, as shown in Fig. 5. The molecules were allowed to relax after switching OFF the driving voltage pulse, as shown in Fig. 5(a). After the field was switched OFF, the retardance changed by a half-wave in about 34 ms (fall time), which is the time to reach first minima in Fig. 5(a). The time required for the consecutive half-waves of the stroke was increased. The molecules near the surface switched over faster than those in the rest of the device. The final half-wave of the stroke required 1.4 s [final fall time to low state (OFF)] to relax. The rise time was measured after driving the device from the low state to the high state, as shown in Fig. 5(b). The field was switched ON to 3.12 V_{rms} from 0 V_{rms}

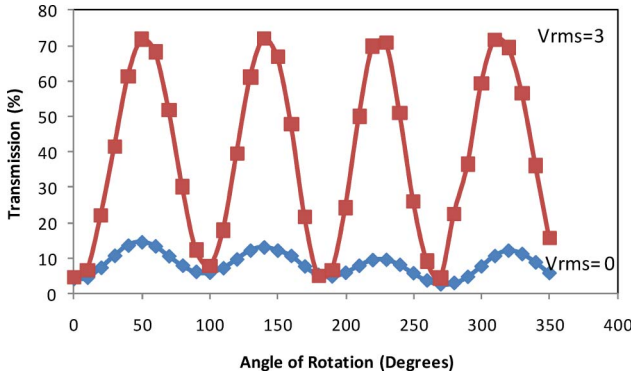

Fig. 4. (Color online) Transmission of the device with respect to angle of rotation at two different voltages: 0 and 3 V_{rms}.

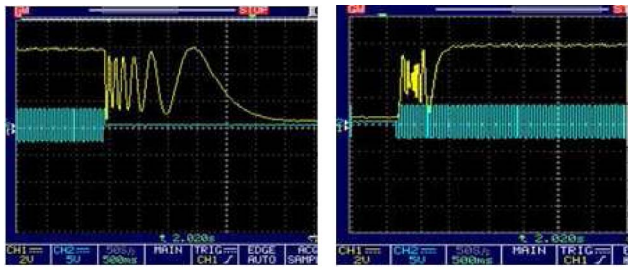

(a) (b)

Fig. 5. (Color online) (a) Device switched OFF from 3.12 to 0 V_{rms} and (b) switched ON from 0 to 3.12 V_{rms} (upper trace, optical response; lower trace, electrical signal).

using the driver electronics without any holding voltage. The time required for the retardance to change to half-wave was 36 ms (rise time) immediately after the device was switched ON. The consecutive rise time increased with a final value about 335 ms [final rise time to high state (ON)].

The rise time and fall time were measured to calculate response time (rise time + fall time) of the device after giving a holding voltage using the driver electronics. The nanophotonic device was switched from voltage levels corresponding to different maxima and minima in the T–V characteristics (Fig. 3) to study variation in the response time. We then used a holding voltage and a transition voltage to switch the device ON and OFF, corresponding to different voltage levels, to improve the response time. Figure 6 shows a transition from 4.7 to 8.5 V_{rms}, where 4.7 V_{rms} was used as the holding voltage. Figure 7 shows the response time of the device for different holding and transition voltages. Response time of the device varied from 3.1 s to 43 ms. The minimum response time is 43 ms for the 4.7 to 8 .5 V_{rms} transition, where 4.7 V_{rms} is the holding voltage. The response time was also measured for a LC cell (without CNT electrodes) with the same thickness (20 μm) as the nanophotonic device to find the effect of nanotube electrodes in the switching speed of LCs. Response time of the LC cell

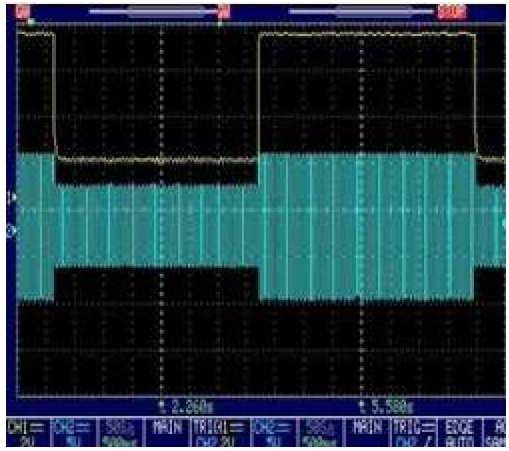

Fig. 6. (Color online) Device switched ON from 4.7 to 8 .5 V_{rms}, with 4.7 V_{rms} as the holding voltage (upper trace, optical response; lower trace, electrical signal).

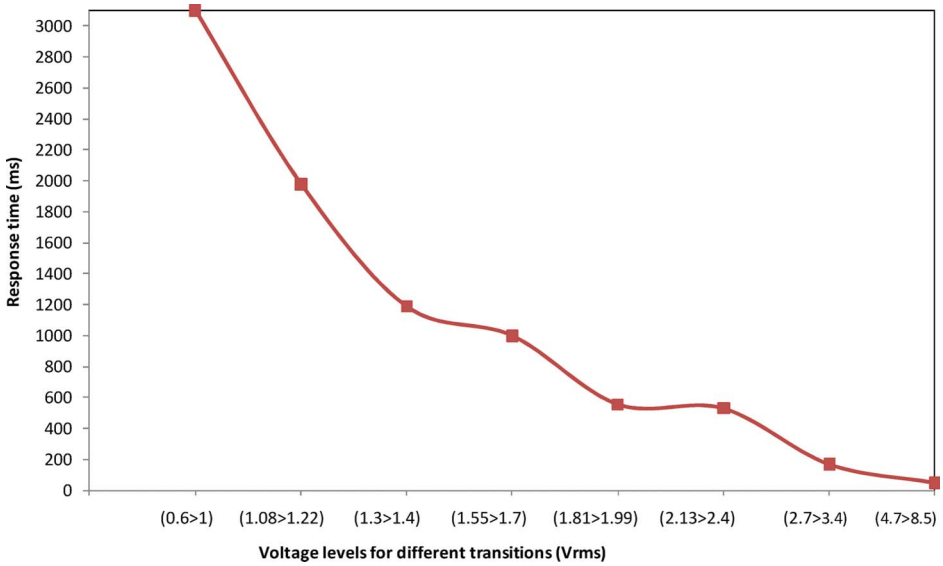

Fig. 7. (Color online) Response time with respect to different voltage transitions.

varied from 3.8 s to 100 ms for different transitions. It was observed that the nanotube electrodes slightly improve the response time of LC molecules because the nanotube electrodes reduce effective thickness and also spawn more electric field due to a large aspect ratio. The difference in light intensity was measured when the device was ON and OFF to measure contrast ratio. Figure 8 shows the contrast ratio measured for the different holding and transition voltages. The contrast ratio is 5.4 for the transition 4.7 to 8.5 V_{rms}. This transition, which has improved response time and contrast ratio, can be used for display-related applications. The response time can be further enhanced by tuning the thickness of the device and the contrast ratio by giving an alignment to the bottom layer because the current alignment of the device is hybrid. The fabricated device has a resolution of over 1000 × 1000 lenslets and a size of 10 mm × 10 mm. The nanotube electrodes can be realized as pixels to make high-density pixel arrays for various photonic applications. The fringing field effect in such systems can be reduced with a suitably patterned top electrode along with vertically grown CNT bottom electrodes.

3. Optical Phase Profile of the Device

The phase profile of the device was retrieved using a Fourier transform technique [13–15]. An interference setup attached to an optical microscope was used to obtain interference fringes from the transparent nanophotonic device. Figure 9 shows interference fringes from four lenslets and the two-dimensional unwrapped phase of a single lenslet at 0.98, 2, and 3.5 V_{rms}. The fringes were observed at 0 V_{rms} due to the alignment of LC molecules by CNT, even though the top electrode was given a planar alignment. The interference fringes were more or less circular and clear at lower voltages [9,16]. As the

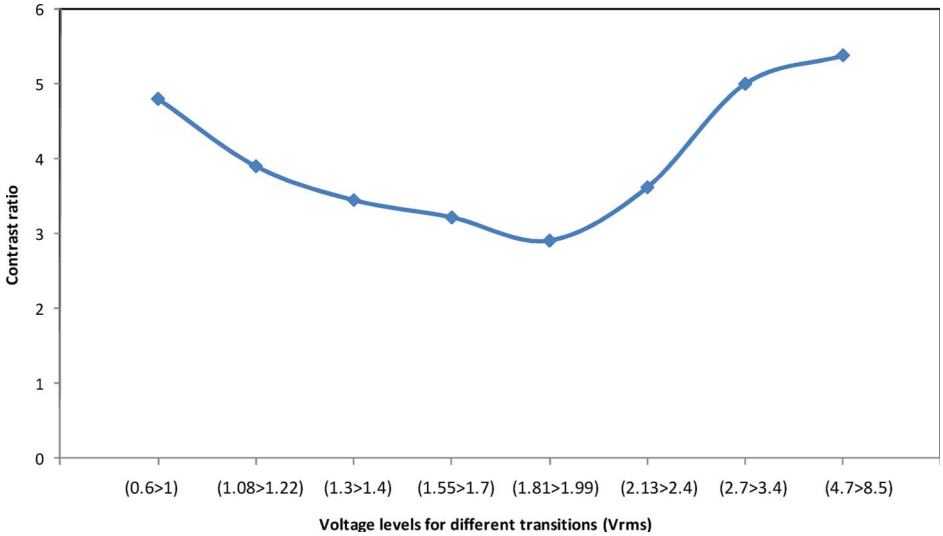

Fig. 8. (Color online) Contrast ratio of the device with respect to different voltage transitions.

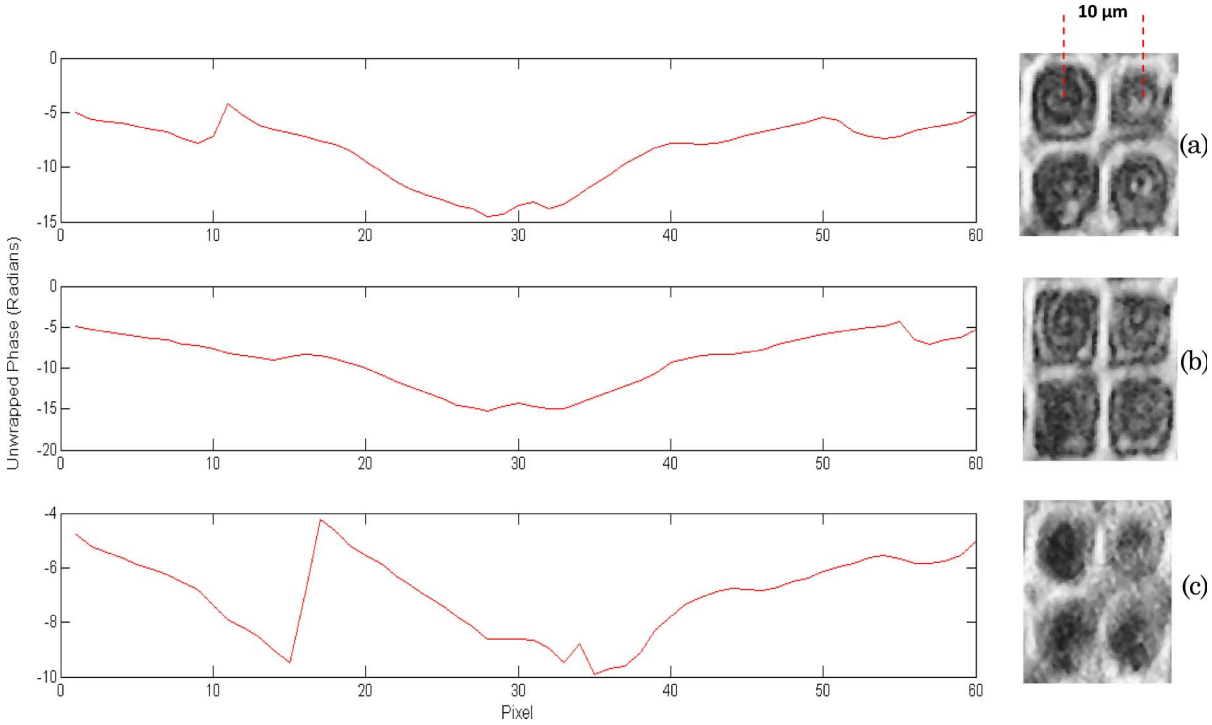

Fig. 9. (Color online) Unwrapped phase of a single lenslet and interference fringes from the nanophotonic device (four lenslets) at (a) 0.98 , (b) 2 , and (c) 2.5 V_{rms}.

voltage increased, the circular fringes became rectangular in shape due to repulsion of electric field from each CNT groups. The fringes started to disappear around 2.5 V_{rms} and we observed a black spot at each lenslet position. The phase modulation is 2.86π at 0.98 V_{rms} with distorted phase profile. The phase profile becomes smooth and parabolic, like at 2 V_{rms}, with phase modulation of $3.5\,\pi$. The phase modulation decreases and the phase profile starts to distort as the voltage increases. The focal length of each lenslet was calculated using the equation [9,16]

$$f = \frac{\Gamma^2}{2\mathrm{OPD}},$$

where OPD is the peak-to-valley optical path difference from the center to the edge of the hybrid grating lenslet and Γ is the radius of the test area ($5\,\mu$m). The focal length was $10\,\mu$m at 0 V_{rms} and increased to $35\,\mu$m at 3 V_{rms}. Further increase in the voltage distorted the orientation of LC molecules in the device and, hence, no focusing was observed. The nanophotonic device acts like a voltage reconfigurable microlens array at lower voltages. The phase profile across the device was voltage reconfigurable and that can be used for hologram applications. A complex hologram can be displayed in the device due to the complex voltage reconfigurable refractive index profiles attainable in the device. From the electro-optic analyses and interference experiments it was concluded that the device's applications can be divide into two regimes, namely, low voltage and high voltage regimes. The response time and contrast ratio of the nanophotonic device is better at higher voltages and can be used for display applications. But the phase modulation is found maximum with a smooth paraboliclike phase profile at lower voltages, which could find application as a voltage reconfigurable microlens array, in holograms, and in other phase-modulating applications.

4. Future Device Developments and Conclusions

This paper presented the electro-optic characteristics of a transparent nanophotonic device fabricated with multiwall CNTs as electrode sites on a quartz substrate covered with nematic LCs. The multiwall CNTs acted as individual electrode sites that spawn an electric-field profile, dictating the refractive index profile within the LC and, hence, creating a voltage reconfigurable optical element. The transmission voltage characteristic, response time, and the contrast ratio were studied to optimize the device's performance. The analyses show that the device has applications as a microlens array, a reconfigurable hologram, and a grating at lower voltages, in addition to the suitability of the device for display applications at higher voltages. The phase profile of the device was retrieved to study the voltage-dependent phase modulation capabilities of the device. The device modulated light up to $3.5\,\pi$.

The nanotube electrodes can be realized as pixels to make submicrometer pixels with matrix addressing for high-resolution display applications using the nanophotonic device, because a device with a size of 10 mm × 10 mm has over 1000 × 1000 phase modulating elements. The density of nanotube electrodes can be further increased by growing nanotubes in

submicrometer separation to address the LC molecules. The fabrication of such a device is in progress.

The authors thank Stephen Morris, Damian Gardiner, Philip Hands, Christoph Bay, Haider Butt, Kanghee Won, and Jon Freeman for fruitful discussions. R. Rajasekharan especially thanks UK-India Education and Research Initiative (UKIERI, British Council) and Cambridge Commonwealth Trust (CCT) for the Ph.D. scholarship.

References

1. C.-Y. Huang, Y.-G. Lin, and Y.-J. Huang, "Switching of vertical alignment liquid crystal cell doped with carbon nanotubes," Jpn. J. Appl. Phys. **47**, 6407–6409 (2008).
2. W. Lee, C.-Y. Wang, and Y.-C. Shih, "Effects of carbon nanosolids on the electro-optical properties of a twisted nematic liquid-crystal host," Appl. Phys. Lett. **85**, 513 (2004).
3. M. D. Lynch and D. L. Patrick, "Organizing carbon nanotubes with liquid crystals," Nano Lett. **2**, 1197–1201 (2002).
4. C. Y. Huang, W. Y. Jhuang, and C. T. Hsieh, "Switching of polymer-stabilized vertical alignment liquid crystal cell," Opt. Express **16**, 3859–3864 (2008).
5. O. Trushkevych, N. Collings, T. Hasan, V. Scardaci, A. C. Ferrari, T. D. Wilkinson, W. A. Crossland, W. I. Milne, J. Geng, B. F. G. Johnson, and S. Macaulay, "Characterization of carbon nanotube–thermotropic nematic liquid crystal composites," J. Phys. D **41**, 125106 (2008).
6. S. J. Jeong, P. Sureshkumar, K.-U. Jeong, A. K. Srivastava, S. H. Lee, S. H. Jeong, Y. H. Lee, R. Lu, and S.-T. Wu, "Unusual double four-lobe textures generated by the motion of carbon nanotubes in a nematic liquid crystal," Opt. Express **15**, 11698 (2007).
7. T. D. Wilkinson, X. Wang, K. B. K. Teo, and W. I. Milne, "Sparse multiwall carbon nanotube electrode arrays for liquid-crystal photonic devices," Adv. Mater. **20**, 363–366 (2008).
8. W. I. Milne, K. B. K. Teo, M. Chhowalla, G. A. J. Amaratunga, S. B. Lee, D. G. Hasko, H. Ahmed, O. Groening, P. Legagneux, L. Gangloff, J. P. Schnell, G. Pirio, D. Pribat, M. Castignolles, A. Loiseau, V. Semet, and V. T. Binh, "Electrical and field emission investigation of individual carbon nanotubes from plasma enhanced chemical vapour deposition," Diamond Relat. Mater. **12**, 422–428 (2003).
9. R. Ranjith, H. Butt, and Timothy D. Wilkinson, "Optical phase modulation using a hybrid carbon nanotube-liquid-crystal nanophotonic device," Opt. Lett. **34**, 1237–1239 (2009).
10. S.-T. Wu, U. Efron, and L. D. Hess, "Birefringence measurements of liquid crystals," Appl. Opt. **23**, 3911–3915 (1984).
11. C. Ruslim and K. Ichimura, "Photocontrolled alignment of chiral nematic liquid crystals," Adv. Mater. **13**, 641–644 (2001).
12. U. Efron, S. T. Wu, and T. D. Bates, "Nematic liquid crystals for spatial light modulators: recent studies," J. Opt. Soc. Am. B **3**, 247–252 (1986).
13. C. Roddier and F. Roddier, "Interferogram analysis using Fourier transform techniques," Appl. Opt. **26**, 1668–1673 (1987).
14. W. W. Macy Jr., "Two-dimensional fringe-pattern analysis," Appl. Opt. **22**, 3898–3901 (1983).
15. M. Takeda, H. Ina, and S. Kobayashi, "Fourier-transform method of fringe-pattern analysis for computer-based topography and interferometry," J. Opt. Soc. Am. **72**, 156–160 (1982).
16. H. Ren, D. W. Fox, B. Wu, and S. T. Wu, "Liquid crystal lens with large focal length tunability and low operating voltage," Opt. Express **15**, 11328–11335 (2007).